SPE-214163-MS

Numerical Investigation of Hybrid Carbonated Smart Water Injection (CSWI) in Carbonate Cores

Anas Mohammed Hassan, Emad W. Al-Shalabi, and Bisweswar Ghosh, Department of Petroleum Engineering, Khalifa University of Science and Technology, UAE; Bennet N. Tackie-Otoo and Mohammed Abdalla Ayoub, Department of Petroleum Engineering, Universiti Teknologi PETRONAS, UTP, Malaysia; Imad A. Adel, Department of Petroleum Engineering, Khalifa University of Science and Technology, UAE

This paper was prepared for presentation at the Gas & Oil Technology Showcase and Conference held in Dubai, UAE, 13 - 15 March, 2023.

Abstract

Carbonated smart water injection (CSWI) is a potential hybrid EOR technology under development. The process involves dissolving CO_2 in smart water ripping the benefits of the synergic effect of CO_2 injection and smart water. Based on the experimental laboratory data, including core flood experiments, this paper presents numerical investigations of the combined impact of dissolving carbon dioxide (CO_2) in smart water (SW) on oil recovery in carbonate cores. An advanced processes reservoir simulator was utilized to build a core-scale model. Both the physics of smart water flooding as well as CO_2-gas injection were captured. The generated model was validated against the coreflooding experimental data on hybrid CSWI, including cumulative oil production (cc) and oil recovery factor (%). The Corey's correlation relative permeability model was used for capturing the multiphase flow. The numerical model was used to understand the underlying recovery mechanisms and crude oil-brine-rock interactions during CSWI. The model was further utilized to perform sensitivity analysis of different parameters and to optimize the CSWI design.

Based on the numerical results, the experimental coreflooding data were accurately history-matched using the proposed model with a minimal error of 8.79% applying the PSO-based optimization method. Moreover, this history-matched model was further used for sensitivity analysis and optimization of the CSWI process. The objective functions for sensitivity analysis and optimization are based on minimizing the history-matching global error and maximizing oil recovery. The optimized design was achieved by performing a sensitivity analysis of various input parameters such as oil and water saturations (S_{oi} and S_{wi}), DTRAP (i.e., relative permeability interpolation parameter). On the other hand, in terms of maximizing the oil recovery while minimizing the usage of injected CSW solutions during CSWI, the optimal solution via the PSO-based approach achieved a cumulative oil recovery of 55.5%. The main mechanism behind additional oil recovery with CSW is due mainly to wettability alteration and ion exchange between rock and brine. Additionally, CSWI was found to be more efficient in releasing trapped oil compared to waterflooding, indicating the synergic effect of dissolved CO_2 in SW solutions. Based on this research, the envelope of CSWI application in carbonates for CO_2-storage is expected to expand. This study presents one

of the few works on numerical modeling of the CSWI process and capturing its effects on oil recovery. The optimized core-scale model can be further used as a base to build a field-scale model. This promising hybrid CSWI process under optimum conditions is expected to be economical and environmentally acceptable, which promotes future field projects.

Introduction

The crude oil preserved in carbonate reservoirs represents approximately 60% of the global oil reserves and the world's total oil production (Akbar *et al.*, 2000). Oil recovery from carbonates can be exceptionally arduous compared to sandstone formations (Chavan *et al.*, 2019). Due to its fractured character and oil-wetting nature, carbonate reservoirs typically have low oil recovery factors (Chilingar and Yen, 1983; Aljuboori *et al.*, 2019).

Accordingly, tremendous efforts have been focused to enlaced oil production from these reservoirs. This is supported by the fact that the demand on crude oil is expected to remain sizeable in the future. According to the prediction of the International Energy Agency (IEA) in 2040, approximately 30% of the world's energy demand will be fulfilled by crude oil (IEA, 2020 and 2021). Moreover, climate change concerns have caused a reduction in explorations for new large oil and gas (O&G) reserves (Bai and Xu, 2014). Consequently, the importance of aged (carbonate) reservoirs in sustaining the global supply of O&G demand has become greatly growing (Akbar *et al.*, 2000; Alvarado and Manrique, 2010). Therefore, enhanced oil recovery (EOR) is to play key role in O&G production from these matured fields by boosting the overall recovery rate in an efficient and environmentally responsible manner (Hassan *et al.*, 2019). Numerous novel EOR methods have been created and employed to achieve improved water imbibition, interfacial tension (IFT) reduction, better mobility control, and consequently high oil recoveries (Lake *et al.*, 2014; Adil *et al.*, 2023).

Smart/low-salinity water (SW/LSW) injections and carbonated water injection (CWI) are among the most promising and recent EOR techniques (Lager *et al.*, 2008a). The SW/LSW floodings have been studied in laboratories for the past two decades (Webb *et al.*, 2004). In addition, the carbon dioxide injection method at both miscible and immiscible statuses is an established EOR technique that causes oil swelling and viscosity reduction, bulging of the oil blobs, and improved viscous force of the displacing fluid (Yongmao *et al.*, 2004). The majority of the previous studies on SW/LSW suggest that the governing oil recovery mechanism is multicomponent ion exchange (MIE) (Lager *et al.*, 2008b). The MIE mechanism is responsible for altering the initially oil-to-mixed wet reservoir formations (i.e., carbonate and sandstone reservoirs) towards a more water-wetting condition because of the electrically polar crude oil compounds desorbed from the surface of the rock formation. The injected SW/LSW has multivalent ions that get interchanged with cations occurring on the surface of the carbonate rock, which results in the alteration of the rock surface's electrical charge (Yousef *et al.*, 2011). Additional underlying mechanisms of smart-water include IFT reduction, rock dissolution, and electrical double-layer expansion (Morrow, 1991). Nevertheless, they have yet to be universally accepted as the predominant mechanism (Hassan *et al.*, 2022a,b,c,d,e; Hassan *et al.*, 2021; Hassan *et al.*, 2020a,b,c).

The key aspect of an effective impact on the oil-rock-brine interaction by the SW/LSW depends on careful selection and adjustment of the salinity and the ionic composition of the injected brine (i.e., SW/LSW). For instance, sulfate-enriched brines have been observed to reduce the oil-water IFT, and the brines containing Mg^{2+} and Ca^{2+} can coalesce with the oil droplets more effectively (Ayirala *et al.*, 2019). Moreover, the sulfate ion initiates a good ionic reaction on the rock surface and dissolves the surface to roughen it, owing to the sulfate-ion being highly reactive on the calcite surface. Moreover, the low salinity and controlled ionic composition brine can favorably change the contact angle of the oil droplet on the oil-wet rock surface towards more water-wetness. Ayirala *et al.* (2020) observed that the coalescence of the oil-brine interface initiated by Mg^{2+} and Ca^{2+} ions is more efficient when compared to SO_4^{2-} ions. Also, it was reported that injecting low salinity water into the rock can change the crude oil composition through the formation of water micro-dispersions in the oil phase. Water micro-dispersion in the oil results in greater sweep efficiency due to oil swelling. However, the recovery improvements by seawater injection is attributed to a change in IFT, leading to greater surface dilatational elasticity (Tetteh and Barati, 2019).

In the last few decades, miscible CO_2 injection has contributed to a significant volume of oil recovery (Adil *et al.*, 2018a and b). On the other hand, recent investigations show that the benefits of injecting CO_2 dissolved in water have greater advantages over injecting CO_2 as a supercritical fluid (Zhang *et al.*, 2019a and b). Thus, as a result of the highly favorable mass transfer mechanism, oil recovery using the CWI can be more efficient in terms of reducing oil viscosity, oil swelling factor, and creating higher viscous forces than CO_2 injections alone (Riazi *et al.*, 2009). In addition, better sweep efficiency can be expected in CWI due to less gravity segregation and reduced channeling effects as a result of the increased density and viscosity of the CO_2 dissolved in injected water (Ghosh *et al.*, 2020). Consequently, it can be predicted that the synergic effect of CO_2 dissolved in smart water (i.e., carbonated smart water injection, CSWI) could improve recoverable reserves even more than SW/LSW or CO_2 injections alone (Al-Shalabi *et al.*, 2014 and 2016). The corroborative evidence in this regard can be found in the work of Soleimani *et al.* (2021) where they observed about 5% additional recovery when smart carbonated water was used as displacement fluid compared to the smart water or CO_2 injections alone. Hence, as a result of the significant effect on oil-rock-brine interactions and the operative ease of these two EOR methods (i.e., SW and CWI), it is justified to study them both sequentially and simultaneously and evaluate their potential synergic effect and to investigate the potential synergistic effect of these two techniques sequentially and simultaneously along with the underlying mechanisms by studying the rock-brine-oil interactions (Ghosh *et al.*, 2022). Another advantage of CWI technique is that it does not require a vast amount of CO_2 and more CO_2 can be stored in the subsurface at significantly lower pressures (Sohrabi *et al.*, 2009; Ghosh *et al.*, 2022). Ghosh *et al.* (2022) conducted a series of laboratory corefloods performed at reservoir conditions to investigate the recovery potential of both SW/LSW injection and CWI as well as their individual potential in recovering residual oil using core-plugs and crude oil from a local carbonate reservoir.

Thus, CSWI is a potential hybrid EOR technology that entails dissolving CO_2 in SW/LSW to reap the advantages of the synergic effect of CO_2 dissolved in SW/LSW. Based on the experimental laboratory data of Ghosh *et al.* (2022), this paper presents numerical investigations of the combined effect of CO_2 dissolved in SW/LSW on oil recovery during CSWI in carbonate reservoirs.

Methodology

This contribution represents a numerical modeling study of the innovative hybrid CSWI-based EOR method at the core-scale. The related numerical simulations for this investigation were performed using the Computer Modeling Group (CMG) simulator. The systematic flowchart for this numerical approach using the CMG simulator is shown in Figure 1. The optimum CSWI recovery process was ultimately determined by applying the CMG simulation tools in stages. With the help of an advanced processes reservoir simulator tool, we initially identified the base case solution. The Cartesian grid was constructed to replicate the core settings using the experimental laboratory data (Ghosh *et al.*, 2022), after which the rock and fluid parameters were determined. Thereafter, the rock-fluid dataset was used to create the PVT (i.e., pressure, volume, and temperature) table, which accounted for the initial reservoir conditions in regards to pressure, saturation, and temperature. Subsequently, we obtained the base case solution data by running the advanced processes reservoir simulator tool (i.e., CMG model). Additionally, to enhance the base case results acquired from the CMG model, we carried out sensitivity analysis, history matching, and optimization studies utilizing the optimization tools that are covered in the next sections.

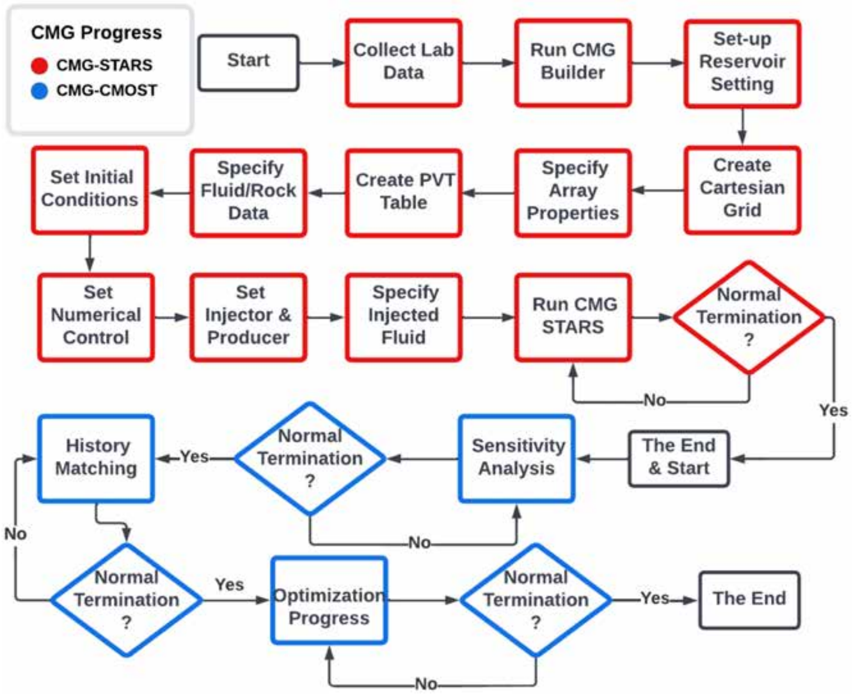

Figure 1—Flowchart for the numerical approach using the CMG-simulator for the carbonated smart water injection (CSWI) process at the core-scale.

Advanced Processes Reservoir Simulation.

The advanced processes reservoir simulation tool (i.e., CMG simulator) is proficient in reproducing and modeling advanced recovery processes that involve injections of gas, solvents, air, and chemicals (Zhang *et al.*, 2019; Kumar and Mandal, 2020). The advanced processes reservoir simulator is characterized by a finite difference numerical simulator that can resolve a series of conservation equations, such as the material balance, heat exchange, chemical processes, phase equilibrium, and flow equations. Furthermore, the fundamental governing equations for the elementary volume (i.e., the region of interest) are related to mass and energy conservation. The configuration for each component in the elementary volume is associated with the inflow and outflow of injected fluids in the region of interest, which is the core-sample (Liu and Chen, 2018).

Moreover, the advanced processes reservoir simulator uses many different relationships in addition to the fundamental conservation equations, with Corey's correlation (Corey, 1977) serving as the primary association. With the help of Cory's correlation, relative permeability curves will be created, summarizing the data on fluid-rock (e.g., crude oil-brine-rock, COBR) interactions. The injection of the chemical solution during the CSWI-based EOR process causes changes in the aqueous phase's physicochemical properties, and the advanced processes reservoir simulator interprets different fluid flow behaviors by interpolating relative permeability curves (CMG, 2019). Corey's correlations are given by (Corey, 1977):

$$\mathbf{K_{rw} = K_{rwiro}\left(\frac{S_w - S_{wcrit}}{1.0 - S_{wcrit} - S_{oirw}}\right)^{N_w}} \quad , \tag{1}$$

$$\mathbf{K_{row} = K_{rocw}\left(\frac{S_o - S_{orw}}{1.0 - S_{wcon} - S_{orw}}\right)^{N_{ow}}} \quad , \tag{2}$$

$$\mathbf{K_{rog} = K_{rogcg}\left(\frac{S_l - S_{org} - S_{wcon}}{1.0 - S_{gcon} - S_{org} - S_{wcon}}\right)^{N_{og}}} \quad , \tag{3}$$

$$K_{rg} = K_{rgcl}\left(\frac{S_g - S_{gcrit}}{1.0 - S_{gcrit} - S_{oirg} - S_{wcon}}\right)^{N_g}, \tag{4}$$

where K_{rw} is the water phase relative permeability for the water-oil table, K_{row} is the oil phase relative permeability for the water-oil table, K_{rog} is the liquid phase relative permeability for the liquid-oil table, K_{rg} is the gas phase relative permeability for the liquid-gas table, S_{wcon} is the connate water saturation, S_{wcrit} is the critical water saturation, S_{oirw} is the irreducible oil saturation for the water-oil table, S_{orw} is the residual oil saturation for the water-oil table, S_{oirg} is the irreducible oil saturation for the liquid-gas table, S_{org} is the residual oil saturation for the liquid-gas table, S_{gcon} is the connate gas saturation, S_{gcrit} is the critical gas saturation, K_{rocw} is K_{ro} at connate water saturation, K_{rwiro} is K_{rw} at irreducible oil saturation, K_{rgcl} is K_{rg} at connate liquid saturation, K_{rogcg} is K_{rog}at connate gas saturation, N_w is the exponent for calculating K_{rw} from K_{rwiro}, N_{ow} is the exponent for calculating K_{row} from K_{rocw}, N_{og} is the exponent for calculating K_{rog} from K_{rogcg}, and N_g is the exponent for calculating K_{rg} from K_{rgcl}.

Noteworthy is the fact that the water-oil relative permeability table is produced utilizing the Equations (1) and (2), and the liquid-gas relative permeability table is prepared using Equations (3) and (4). In the advanced processes reservoir simulator, the relative permeability curves' interpolations are used for various fluid flow behaviors that result from modifications in the physicochemical characteristics of the aqueous/gas phase brought on by the presence of chemicals (e.g., CSWI injected fluid).

Model Description.

The CSWI-based EOR procedure was investigated in the laboratory using core-flooding experiments at a reservoir temperature and pressure of 100 (°C) and 2000 (psi), respectively (Ghosh *et al.*, 2022). The laboratory trials on coreflooding were simulated using a 1-D advanced processes reservoir simulation model. According to a grid sensitivity analysis, the 1-D core-model was placed horizontally with 200 gridblocks (200 × 1 × 1) to replicate the experimental scenario. The model included the dimensions of the core sample, which were 6.8 cm in length and 3.8 cm in diameter. Accordingly, the rock parameters, including permeability and porosity, were simulated, and assumed to be homogeneous for all gridblocks based on the measured value of the selected core sample. For fluid properties, the different fluid parameters considered in the simulation model comprise density and viscosity of the aqueous and oleic phases. Table 1 summarizes the numerous input parameters for the model. Finally, one injector well and one producer well were included in the core-scale model (Figure 2).

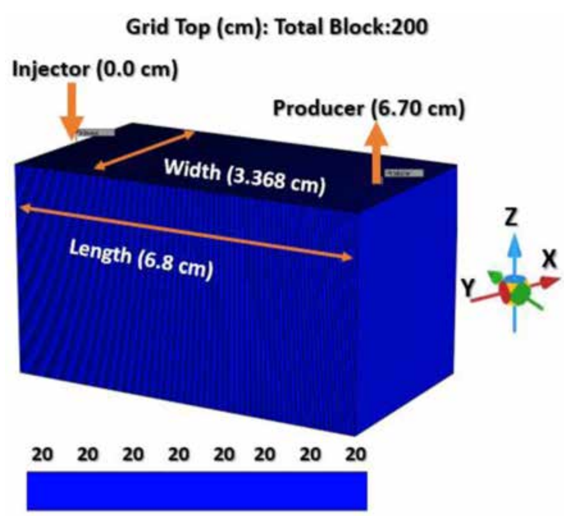

Figure 2—Permeability map for the core model which mimics the rock permeability of 20 milli-Darcy (mD) (i.e., homogenous case study).

Table 1—Rock and fluid properties of the core-model used

Rock Properties	Value	Fluid Properties	Value
Gridblock Number	200	Water Viscosity (cP)	1.00
Core Model Dimensions (cm)	6.8 × 3.368 × 3.368	Water Density (g/cm^3)	1.03
Gridblock Dimensions (cm)	0.034 × 3.368 × 3.368	Stock Tank Oil Gravity (API)	40.6
Kx, Ky, Kz (mD)	20	Oil Viscosity (cP)	4.28
Φ (%)	22	Oil Density (g/cm^3)	0.8694
Reservoir Pressure (psi)	2000	Initial Oil Saturation	0.68
Reservoir Temperature (°C)	100	Initial Water Saturation	0.32

Optimization Tool.

A sensitivity analysis, history matching, and optimization studies were carried out by the optimization software. The primary objective of using the optimization software is to improve the base case datasets, which are obtained from the advanced processes reservoir simulator and comprise of measured and assumed values. Numerous variables, such as oil and water saturations (So and Sw), relative permeability, and water chemistry (i.e., the concentration of SW and CWI), must be taken into account for the CSWI-based EOR technique.

Sensitivity Analysis.. To highlight the effect of different input parameters on the simulation results, a sensitivity analysis was performed utilizing the optimization software. This includes parameters with the most influential effect on the production profile. The latter would facilitate the following processes of history matching and optimization (Zainal *et al.*, 2008; Douarche *et al.*, 2014). As shown in Table 2, the sensitivity analysis started with thirteen alternative parameters. We evaluated the effects of these parameters on decreasing the global error and maximizing the oil recovery profiles observed in the base case outcomes.

Table 2—Defined baseline (default) values for the selected simulation inputs

Parameter Name	Default Value	Parameter Name	Default Value
DTRAP	0.0096	Porosity	0.22
K_{RGCL}	0.8	Prod BHP (KPa)	13789.514
K_{ROCW}	1	S_{GCRIT}	0.05
N_G	2	S_{ORG}	0.1
N_{OG}	2	S_{ORW}	0.3
Perm V	20	S_{Oi}	0.68
Perm H	20	S_{Wi}	0.32

Originally, the response surface methodology (RSM) method was used to perform the sensitivity analysis (Zerpa *et al.*, 2007). RSM is employed to study the correlations between the input parameters and objective functions. The fundamental idea defining RSM is to build a proxy model through a series of planned experiments that may be used to replicate the actual, complex reservoir simulation model. Two different forms of proxy models, i.e., the polynomial regression and the neutral network using the radial basis function (RBF) were considered. The most prevalent form of proxy model is designated as the polynomial regression, which is either in linear or quadratic forms, and is as given below:

$$y = a_o + \sum_{j=1}^{k} a_j x_j + \sum_{j=1}^{k} a_{jj} x_j^2 + \sum_{i<j} \sum_{j=2}^{k} a_{ij} x_i x_j \quad , \tag{5}$$

where a_o denotes the intercept, a_1, a_2 … …. a_k denote the coefficients of the linear terms, a_{jj} stand for the coefficients of the quadratic terms, and a_{ij} denote cross (interaction) terms coefficients.

The definition of a radial basis function i.e., RBF neural network can be given as a single-layer network radial basis function with an input layer of source nodes, a single hidden layer of nonlinear processing units, and an output layer of linear weights. This mapping of input and output accomplished using an RBF network is expressed as follows:

$$\tilde{y}(x_p) = w_o + \sum_{i=1}^{M} w_i \varphi(x_i x_p) \quad , \tag{6}$$

where $\varphi(x_i x_p)$, x_i, x_p and $\tilde{y}(x_p)$ denote the N-dimensional parameter space, while M denotes the training data size.

History Matching Study.. The objective function of a history matching method is to minimize the errors among the experimental and the simulation cumulative oil data, which is then expressed through the global error percentage. The history matching for the experimental data was performed using the optimization tool, whereby 500 models were simulated with different permutations of the base model's parameter values that were originally presumed. The proprietary optimizer of CMG used particle swarm optimization (PSO), and Designed exploration and Controlled Evolution (DECE) to produce diverse values for the parameters. The model was deemed validated if there was minimal discrepancy between the simulated and experimental results. For history matching through the PSO technique, the experimentally obtained data from the coreflood are compared to those produced from the simulation, as shown in Figure 3.

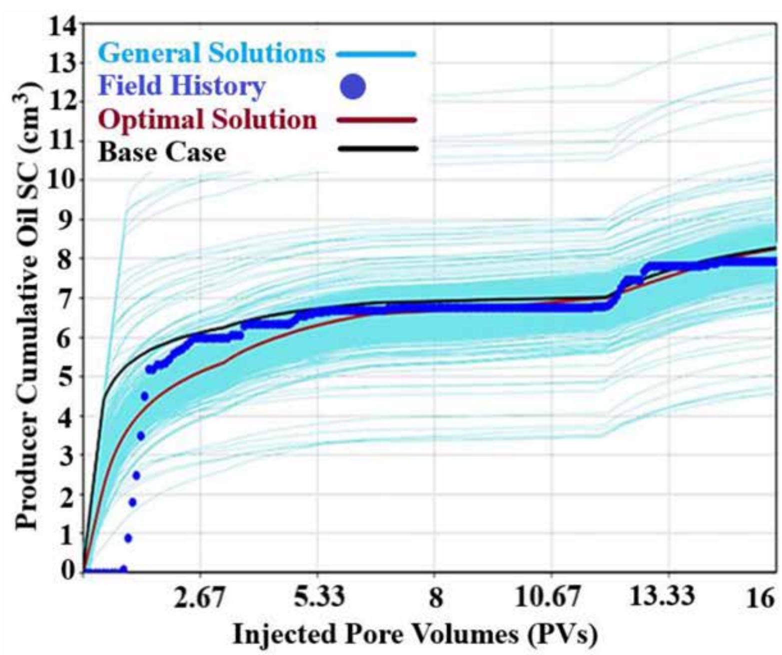

Figure 3—History matching results by Particle Swarm Optimization (PSO) approach.

Optimization Process.. Following the history matching step, the optimization procedure was carried out using the PSO and DECE, which are the proprietary optimizers by CMG. The PSO is the technique that is most typically employed in an optimization procedure. The PSO i.e., the population-based stochastic optimization technique was designed by adopting principles from the social behaviors of fish schools and flocks of birds (AlSofi and Blunt, 2011; Alkhatib and King, 2014). Maximizing the oil recovery factor is the primary objective of the optimization process, while the velocity and position updates are the main operators of PSO. The fundamental steps of the PSO algorithm are outlined in the ensuing five phases (CMG, 2019), which include (i) Swarm initialization via the solution space, (ii) Evaluation of every particle's aptness, (iii) Individual updating along with global bests, (iv) Velocity and position updating of every particle, and (v) Move to step 2 and replicate the step until the termination condition is reached, as shown in Figure 1.

Results and Discussion

The coreflood conducted by Ghosh *et al.* (2022) was simulated using the advanced processes reservoir simulator (CMG, 2019). The simulator was utilized to gain insights into the governing relative permeability curves and their associated interpolation parameters, as well as history matching of the coreflood oil recovery data (Hassan *et al.*, 2022c). Figure 4 shows the oil production profiles versus the injected pore volume (PV) for the carbonated smart water injection. The oil production that was obtained from the coreflooding experimental data was plotted as shown in the Figure 4a (Ghosh *et al.*, 2022). On the other hand, Figure 4b, compares the coreflooding experimental oil production to the simulation model results where there is a notable disparity.

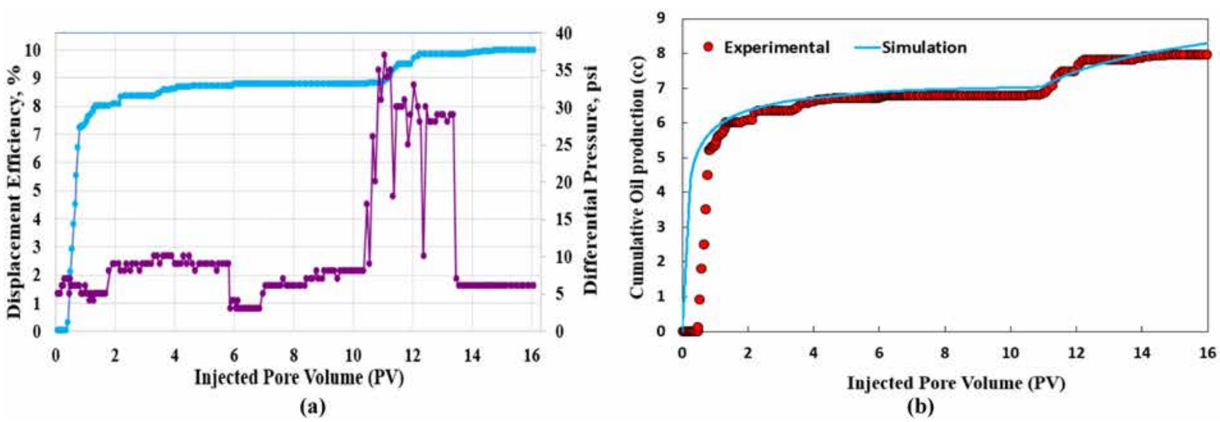

Figure 4—The oil recovery production of the carbonated smart water injection (CSWI) versus the injected pore volume (PV); (a) coreflooding experimental oil recovery data (Ghosh *et al.*, 2022) (b) Comparing the coreflooding experimental oil recovery data to the simulation oil recovery results (i.e., the base case).

Sensitivity Analysis Results.

Sensitivity analysis is the first major function accomplished with the optimization software. Through the sensitivity analysis, the objective is to comprehend how the various simulation model inputs affect the simulation outcomes, minimize the history matching error, and maximize the oil recovery profile. Around thirteen input parameters were chosen and defined in the optimization software's input parameters for this evaluation, as Table 2 enlists. In the optimization tool, the proxy model specifies each effect's sensitivity on the simulation results (e.g., oil recovery production data). The benefit of the proxy model also includes the generation of additional rapid forecasts like computational cost reduction without additional simulation. The proxy models are also useful in certain proxy-based optimization algorithms for rapidly finding an optimal solution (Horowitz *et al.*, 2010). However, the proposed proxy model needs to be validated. The results of the verification plots are shown in Figure 5 using radial basis function (RBF) neural network proxy models, since it provides accurate results (Hassan *et al.*, 2023).

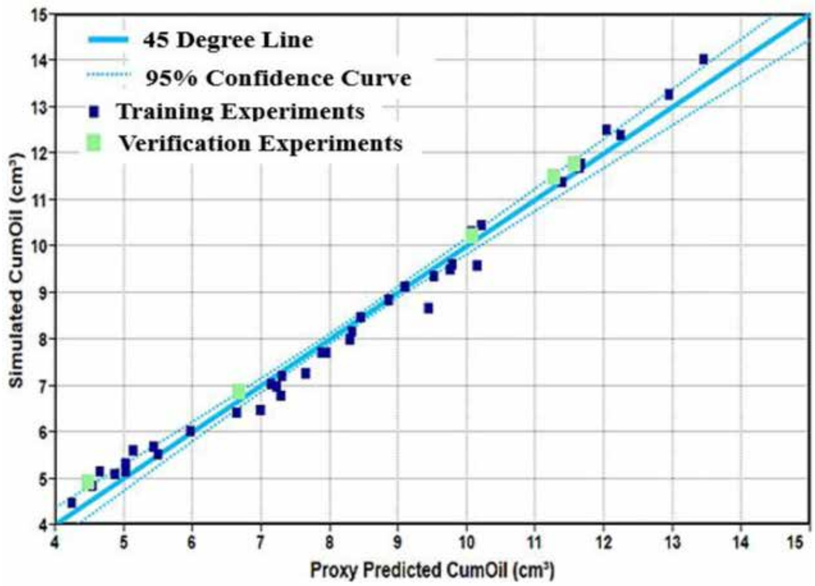

Figure 5—The verification plot for radial basis function (RBF) neural network proxy model.

Moreover, the standard one parameter at a time (OPAAT) approach was used to conduct another sensitivity analysis with the aim of evaluating the impact of input parameters on cumulative oil production (i.e., conventional approach) (CMG, 2019). This strategy seeks to identify each parameter's impact by changing just one parameter at a time. The results of this analysis are shown as a Tornado-plot in Figure 6, which illustrates the parameters that influence the oil recovery profiles most. According to the Tornado-plot analysis, the oil saturation (S_{oi}), DTRAP, water saturation (S_{wi}), NOG, SORG, SORW, KRGCL, and SGCRIT have most significant impact on the oil recovery profiles, as shown in Figure 6.

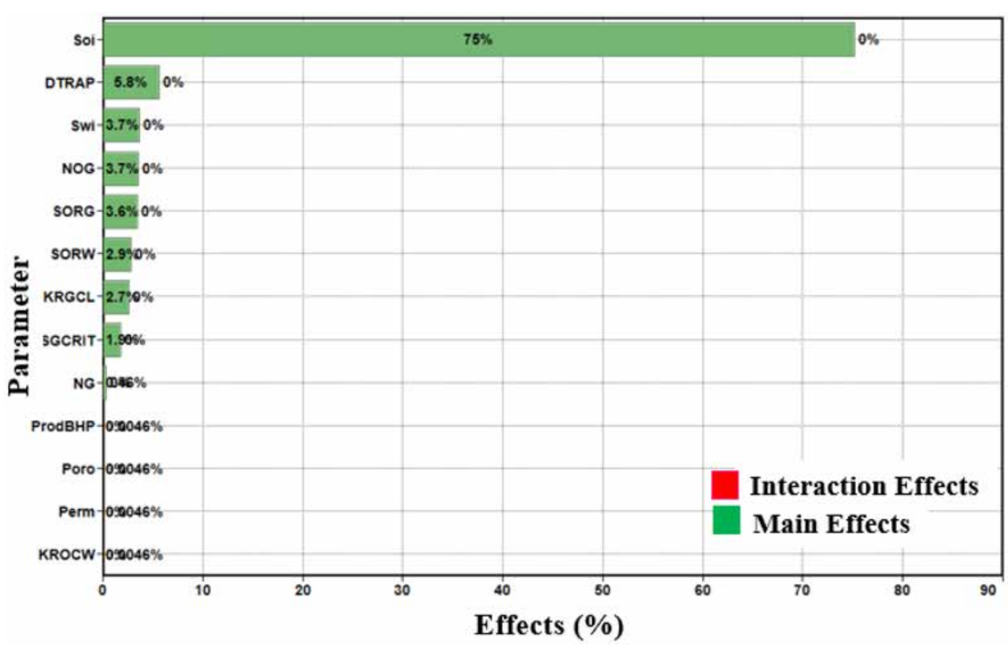

Figure 6—Sensitivity analysis results showing the effect of various parameters on the cumulative oil production using the Tornado-plot method.

Additionally, The SOBOL and MORRIS methods were also applied to derive the findings of the sensitivity analysis. The SOBOL and MORRIS are two recent methods of variance-based sensitivity analysis (Garcia *et al.*, 2019). These techniques carry out the sensitivity analysis across the entire input region, find the non-linear responses, and combine the impacts of each parameter into a core effect and an interaction effect, since O&G reservoir responses are mainly nonlinear. As a result, the analytical process becomes more advanced and requires fewer runs. The outcomes were examined using the SOBOL variance-based sensitivity analysis approach, as seen in Figure 7. The parameters with the most positive influence on the oil recovery profiles during CSWI-based EOR process, as shown by the SOBOL sensitivity analysis plot, are the oil saturation (S_{oi}), SORW, DTRAP, water saturation (S_{wi}), NOG, SORG, KRGCL, and SGCRIT (Figure 7).

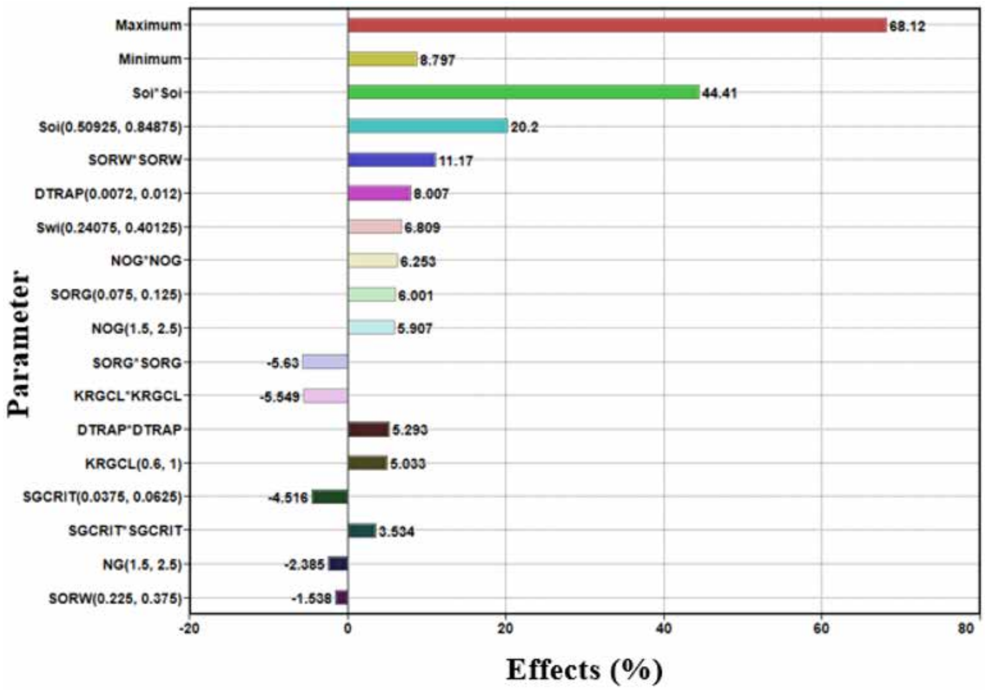

Figure 7—Sensitivity analysis results showing the effect of various parameters on the cumulative oil production using the SBOL method.

Furthermore, Figure 8 shows the outcomes of the MORRIS variance-based sensitivity technique. The MORRIS sensitivity analysis plot displays the parameter values in relation to their impact on improved oil recovery profile. The factors that influence oil recovery profiles most during the CSWI-based EOR process are those that are farthest to the right on the x-axis in the MORRIS plot, as shown in Figure 8. The parameters with the most positive influence on the oil recovery profiles during CSWI-based EOR process, as shown by the MORRIS sensitivity analysis plot, are the oil saturation (S_{oi}), DTRAP, water saturation (S_{wi}), SORG, SORW, KRGCL, SGCRIT, NG, and prod BHP (Figure 8).

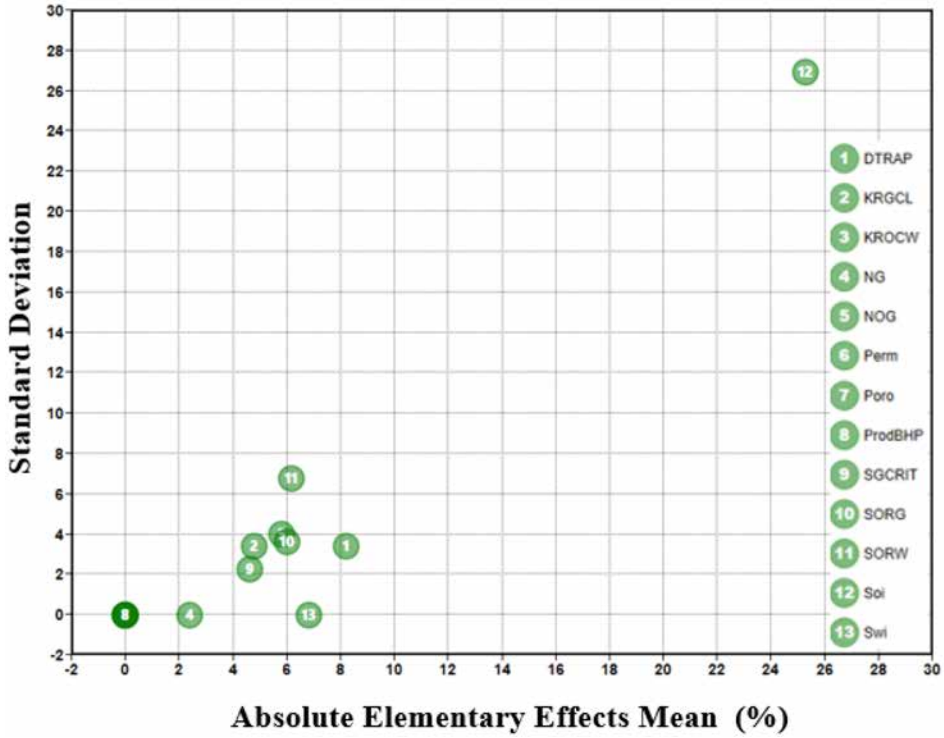

Figure 8—Sensitivity analysis results showing the effect of various parameters on the cumulative oil production using the MORRIS method.

In summary, combining the results of the three-sensitivity analyses identifies numerous common characteristics that have the greatest effects on oil recovery, namely, the oil saturation (S_{oi}), DTRAP, water saturation (S_{wi}), SORG, SORW, KRGCL, NOG, and SGCRIT. Thus, the three sensitivity analysis approaches (i.e., Tornado-plot, SBOL, and MORRIS) show that the relevant parameters are essentially the same in the coreflooding experiments on the CSWI-based EOR process (Ghosh *et al.*, 2022).

History Matching Results.

As elucidated previously, the history matching procedure is an optimization technique for reducing the error between the simulation and experiment data. In order to align the simulation model to the results of the experimental coreflooding, we have simulated 500 models for this study using various input parameter combinations, which involves mismatched error reduction between base case scenario, as depicted in Figure 4b earlier. As revealed in Figure 4b, there is a mismatch between the base case scenario simulation results and the coreflood data. Such a finding suggests that the parameters' presumed values were not sufficiently close to the real experimental conditions. It necessitated additional parameter adjustment to get a better match and find the correct values for the parameters. In order to match the simulation data to the coreflood data in the history matching investigation, we chose the oil recovery as the goal function. The PSO optimizer of the CMG simulator was used to produce the various input parameters.

The experimental IDs of the several models that the optimization engine constructed throughout history match serve as their identifiers. The model was deemed to be validated if its set of parameters differed from the experiment results by the least amount. Figure 9 presents the oil recovery profiles for the coreflooding experimental data, base case model, and history-matched model. The figure demonstrates how the PSO (Particle Swarm Optimization) history-matched model has improved the ability to match the coreflooding experimental data.

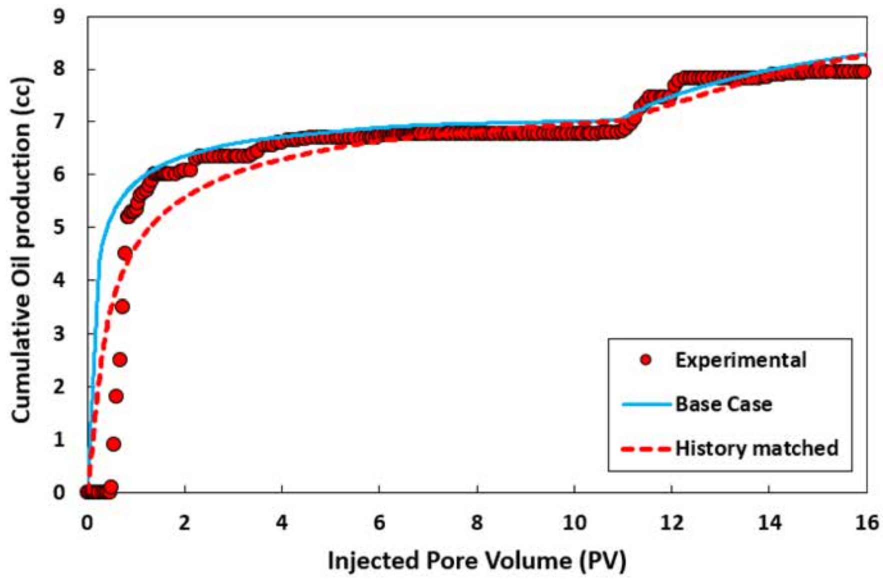

Figure 9—Cumulative oil production (cc) versus injected pore volumes (PV) from simulation and coreflooding experimental results.

Table 3 provides values for several parameters used in the base-case scenario (assumed) and the history-matched scenario when the optimization software was applied (i.e., PSO method). In Table 3, DTRAP is the relative permeability interpolation parameter for CSWI, K_{RGCL} denotes the relative permeability of the gas phase for the liquid-gas table at connate liquid saturation, K_{ROCW} denotes the oil phase relative permeability for a water-oil table at the connate water saturation, Prod BHP represents the bottom hole pressure production rate, S_{ORG} is the residual oil saturation for the liquid-gas table, and S_{oi} and S_{wi} are the oil and water saturations, respectively.

Table 3—Base-case and history matched-case parameters using the optimization software

Parameters	Base Case Values	History Matched Values_PSO
DTRAP	0.0096	0.0079
K_{RGCL}	0.800	0.884
K_{ROCW}	1	1
N_G	2	2.36
N_{OG}	2	1.71
Permeability	20.25	20.25
Porosity	0.2215	0.2215
Prod BHP	13789.51	16202.68
S_{GCRIT}	0.05	0.05
S_{ORG}	0.10	0.12
S_{ORW}	0.30	0.31
S_{oi}	0.679	0.679
S_{wi}	0.321	0.321

Figure 10 illustrates the history matching global error between the simulated and the experimental results for numerous models with different input settings created by the PSO CMG's optimizer model. Figure 10 shows that the PSO history-matched parameter values have the lowest error between the experimental and simulated results among the 500 input value sets (i.e., general solutions). The global error of the PSO history-matched optimum solution is 8.797 % (i.e., as opposed to the base case global error of 13.517 %), as listed in Table 4.

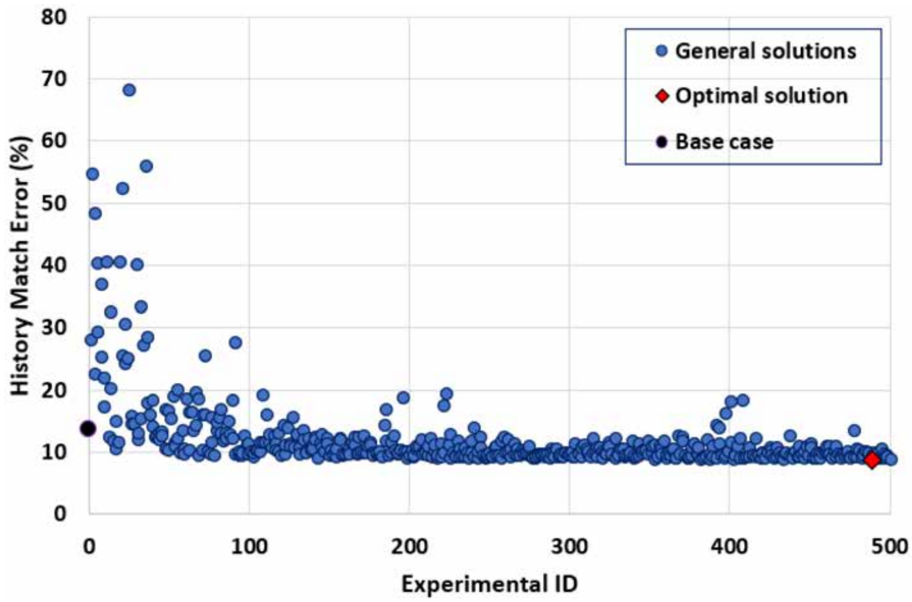

Figure 10—History matching global Error (%) between simulation and experimental data for PSO-based CMG's optimizer model.

Table 4—History matching process results (i.e., global error %) using PSO-based CMG's optimizer model

Optimization Software -Process	Objective Function	Total Runs	Results	
			Base-Case Global Error	Optimal Global Error (PSO)
History Matching	Minimize Global Error (%)	500	13.517%	8.797%

Additionally, Figure 11 shows the corresponding oil production rate (cc/min) profiles produced from the simulated model results using PSO approach against the coreflooding experimental data. In Figure 11, the increase in oil production rate observed at the later part at nearly 11 PVs of the injected CSWI process (i.e., for both simulated and experimental results) are caused by carbonated smart water (CSW) mobility control.

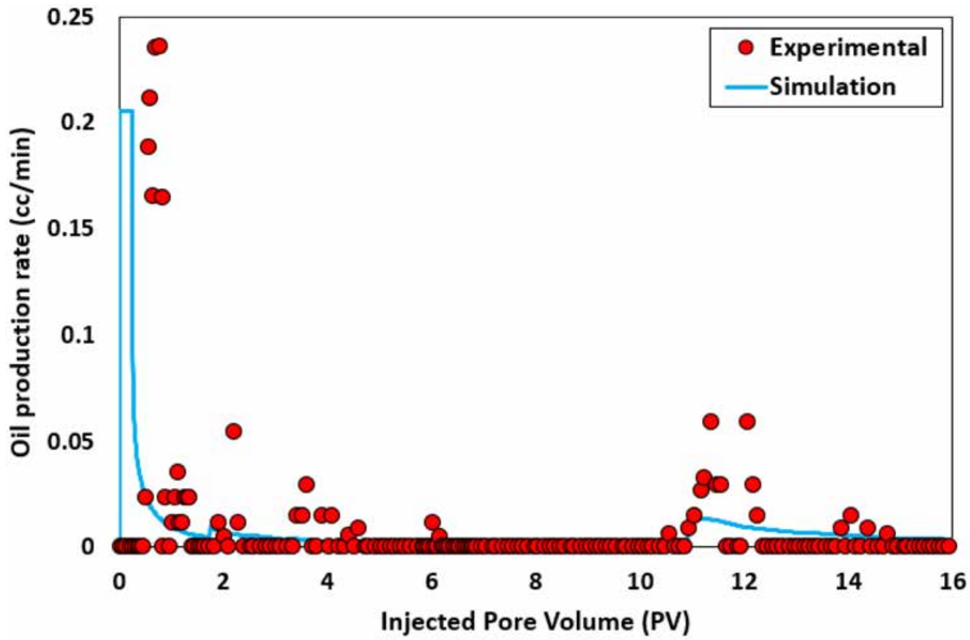

Figure 11—Comparison between simulation and experimental results using PSO approach for oil production rate (cc/min) versus injected pore volume (PV).

Optimization Process Results.

The aim of the optimization procedure is to maximize oil recovery. The number of runs used for the optimization procedure is 500. The optimization algorithm i.e., PSO-based CMG's optimizer model was used to carry out the optimization process. Figures 12a and 12b correspondingly display the optimization process results for the cumulative oil production (cc) and oil recovery factor versus the injected pore volume (PV) using the PSO method. According to Figure 12, the oil production and recovery factor are 8.3 (cc) and 55.5 (%), respectively.

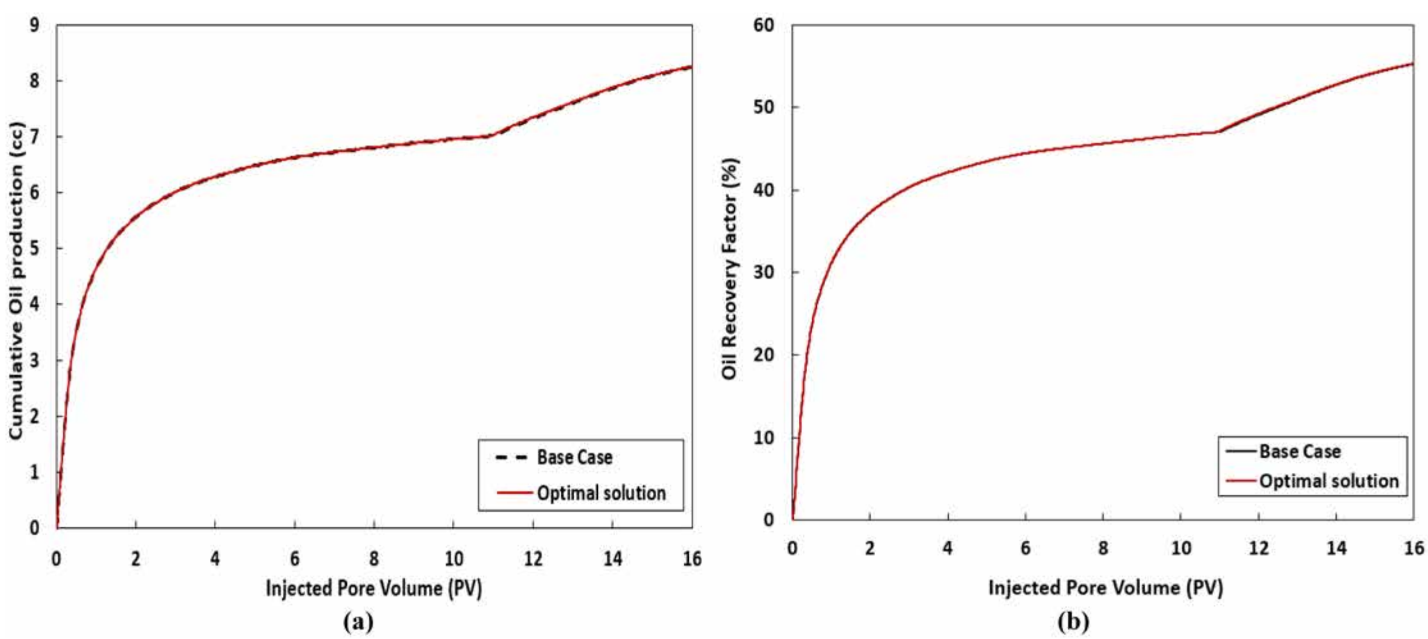

Figure 12—The optimization process using PSO-based CMG's optimizer model (a) Cumulative oil production (cc) vs. injected pore volume (PV) (b) Oil recovery factor (%) vs. injected pore volume (PV).

Additionally, when considering the oil recovery factor, Figure 13 shows the optimization process results produced from the PSO method. The PSO-based optimization process resulted in a base case oil recovery of 55.3% and an optimal oil recovery of 55.5% (i.e., oil initial in place, OIIP). Table 5 summarizes the oil recovery factor results (i.e., optimization process) using the PSO CMG's optimizer model. As stated above, in the CSWI-based EOR method, maximizing oil recovery serves as the optimization's objective function. This implies that the optimal solution via the PSO-based method is preferable (55.5%) to the base case solutions (55.3%) in terms of improving oil recovery profiles.

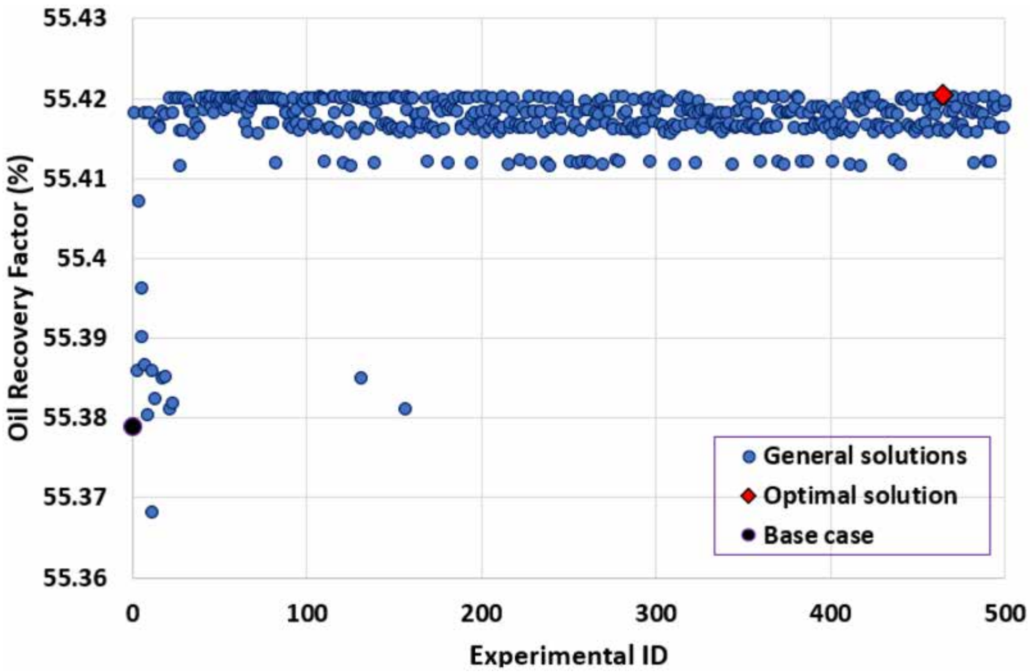

Figure 13—Oil recovery factor (%) versus injected pore volumes (PV) from the optimization process using PSO-based CMG's optimizer model.

Table 5—Optimization process results (i.e., oil recovery factor %) using PSO CMG's optimizer model

Optimization Software -Process	Objective Function	Total Runs	Results	
			Base-Case (PSO)	Optimal (PSO)
Optimization Progress	Maximize Oil Production (%)	500	55.3%	55.5%

Relative Permeability Curve.

The relative permeability curves determining were generated using Corey's correlation to determine the water-oil table's saturation endpoints. Corey's correlations were used together with the DTRAPW (i.e., for the wetting phase) and DTRAPN (for the non-wetting phase), which serve as interpolation parameters (Hassan *et al.*, 2022c). The values of the dimensionless interpolation parameters, with values ranging from 0 and 1, are associated with the capillary number (N_c) as follows (Hakiki *et al.*, 2015):

$$\text{ratw} = \frac{\log_{10}(N_c) - \text{DTRAPWA}}{\text{DTRAPWB} - \text{DTRAPWA}}, \quad (7)$$

$$\text{ratn} = \frac{\log_{10}(N_c) - \text{DTRAPNA}}{\text{DTRAPNB} - \text{DTRAPNA}}, \quad (8)$$

where the interpolation parameters DTRAPWA and DTRAPNA reflect a low capillary number for high IFT values and a high capillary number for ultralow IFT values for the wetting phase, respectively.

In general, we applied multiple sets of relative permeability curves so that the effects of the alterations in wettability caused by smart water (SW) as well as the carbonated smart water (CSW) injections may be incorporated. However, in this study the only interpolation parameter employed was for CO_2 injection because the quantity of the CO_2 dissolved in the CSW solutions causes the relative permeability to alter during the CSWI-based EOR process; Likewise, the varying injection rates of 0.2, 0.4, and 0.5 cc/min were the cause for the distinct increments in oil recovery, which have been demonstrated on the cumulative oil production curve (Figures 12a and 12b). The injection rate preceding the CSWI was 0.5 cc/min, and this same injection rate was also maintained during the CSWI process. The CO_2 dissolved in the smart water during the CSWI-based EOR process is thus responsible for the considerable increase observed in oil production. The relative permeability interpolation implemented the CO_2 mole fraction in the injected smart water to simulate this observed incremental recovery of the OIIP through CSWI process.

Following that Corey's correlation was implemented to generate the relative permeability curves, while the saturation endpoints of the water-oil table were calculated based on the results of the coreflooding experiments (Ghosh *et al.*, 2022). Subsequently, the effects of the CSW solutions on wettability change was included utilizing the sets of relative permeability curves, as shown in Table 6. Figure 14 illustrates the relative permeability datasets used for the PSO-optimized simulation model. Also, Figure 14 exemplifies the relative permeability interpolation sets for CSWI process. In this figure, the solid curves indicate the waterflooding process while the dashed curves demonstrate the increased relative permeability during the propagation of the CSWI process. Thus, this demonstrates the additional impact (i.e., the incremental OIIP) of CSW on relative permeability. Therefore, one can note that CSW affects the wettability of the carbonate core sample.

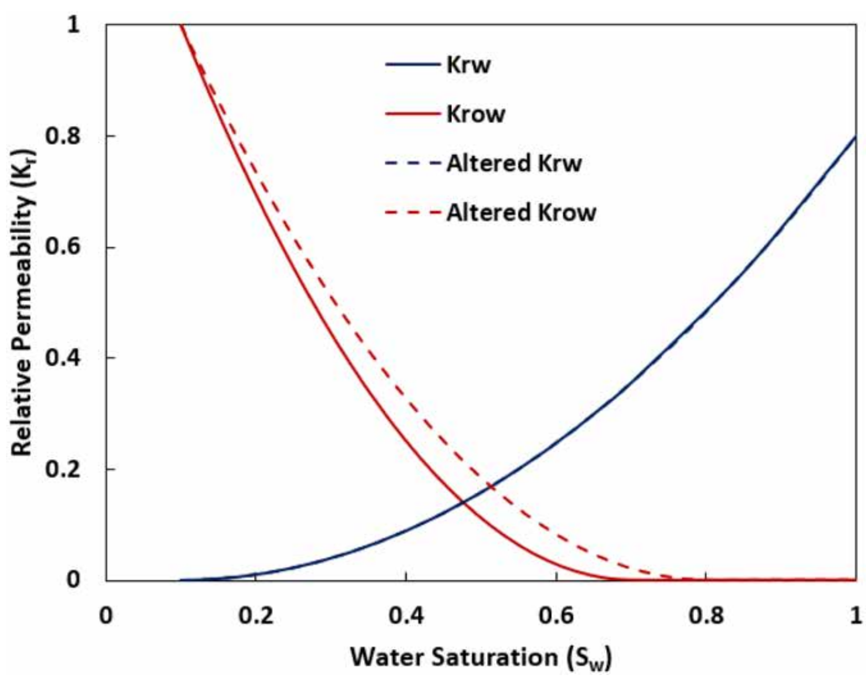

Figure 14—Relative permeability curves used for the carbonated smart water injection (CSWI) process.

Table 6—Interpolation parameters (i.e., DTRAPW and DTRAPN)

Interpolation parameter	Smart Water (SW) Injection (Aqueous Mole Fraction)		Carbonated Smart Water Injection (CSWI) (Aqueous Mole Fraction)	
	Set 1	Set 2	Set 1	Set 2
DTRAPW	-	-	0.0001	0.0096

Interpolation parameter	Smart Water (SW) Injection (Aqueous Mole Fraction)		Carbonated Smart Water Injection (CSWI) (Aqueous Mole Fraction)	
	Set 1	Set 2	Set 1	Set 2
DTRAPN	-	-	0.0001	0.0096

In summary, it is clear evident that the effects of the CSWI causes a significant increase in oil relative permeability, signifying the excellent efficiency of CSW injection in causing wettability alteration of carbonate rocks, leading to augment oil production rate (i.e., up to 55.5 % of the OIIP for the optimized model).

Summary and Conclusions

To acquire greater insights into the mechanisms underlying incremental oil recovery through the hybrid CSWI-based EOR method, we used a core-scale advanced processes reservoir simulation model for this study. The CSWI's procedure entails dissolving CO_2 in smart water (SW) in order to benefit from the advantages of its synergistic effects. In this analysis, the ultimate objective is to gain insight through the effect of CSWI on relative permeability curves in carbonates at reservoir conditions of 100°C temperature. Therefore, initially the optimization software was utilized for conducting the sensitivity analysis to evaluate the effects of several key input parameters included in the simulation models on the simulation results. Next, history matching was performed by tuning certain input parameters derived from the sensitivity analysis with specific coreflooding experimental measurements. At the end, the optimization process was carried out, which involved altering operational controls to attain enhanced oil recovery by means of the recovery factor (%) and the cumulative oil production (cc) being maximized. Through this numerical analysis, the main conclusions may be summarized as follows:

- The experimental coreflooding data were fairly history-matched with a minimum error of 8.79% employing the PSO-based optimization technique.
- Sensitivity analysis methods of tornado-plot, SOBOL, and MORRIS analyses were implemented with objective functions to minimize the history-matching global error and maximize the oil recovery profile.
- The three sensitivity analyses highlighted the most influential parameters to the oil recovery profiles including oil and water saturations (S_{oi} and S_{wi}), DTRAP, S_{GCRIT}, N_O, N_{OG}, K_{RGCL}, K_{ROCW}, S_{ORG}, S_{ORW} and Prod BHP.
- Only one interpolation parameter (i.e., DTRAP) was used in this work was for CO_2 injection since the amount of the dissolved CO_2 in the CSW is the main controller behind the change in the relative permeability during the CSWI-based EOR process.
- Regarding oil recovery optimization during CSWI-based EOR process, the PSO-based optimal solution showed 55.5% oil recovery.

This study presents one of the few works on numerical modeling of the CSWI process and capturing its effect on oil recovery. The optimized core-scale model can be further used as a base to build a field-scale model. This promising hybrid CSWI process under optimum conditions is expected to be economical and environmentally acceptable, which promotes future field projects.

Acknowledgments

The authors wish to thank Khalifa University of Science and Technology (Abu Dhabi, UAE) for providing access to their equipment and facilities. Also, the authors aappreciate Universiti Teknologi PETRONAS (UTP) for their considerable support, which helped accomplish this research.

Nomenclature:

Symbols :	Description
$\boldsymbol{a_o}$	Intercept
$\mathbf{a_1, a_2 \ldots \ldots a_k}$	Linear terms coefficients
$\boldsymbol{a_{jj}}$	Quadratic terms coefficients
$\boldsymbol{a_{ij}}$	Cross (interaction) terms coefficients
K_{rg}	Gas phase relative permeability for liquid-gas table
K_{rgcl}	K_{rg} at connate liquid saturation
K_{ro}	Oil phase relative permeability
K_{rocw}	K_{ro} at connate water saturation
K_{rog}	Liquid phase relative permeability for liquid-oil table
K_{rogcg}	K_{rog} at connate gas saturation
K_{row}	Oil phase relative permeability for water-oil table
K_{rw}	Water phase relative permeability for water-oil table
K_{rwiro}	K_{rw} at irreducible oil saturation
$\mathbf{N_c}$	Capillary number
$\mathbf{N_g}$	Exponent for calculating K_{rg} from K_{rgcl}
$\mathbf{N_{og}}$	Exponent for calculating K_{rog} from K_{rogcg}
$\mathbf{N_{ow}}$	Exponent for calculating K_{row} from K_{rocw}
$\mathbf{N_w}$	Exponent for calculating K_{rw} from K_{rwiro}
S_{gcon}	Connate gas saturation
S_{gcrit}	Critical gas saturation
S_o	Oil saturation
S_{oirg}	Irreducible oil saturation for liquid-gas table
S_{oirw}	Irreducible oil saturation for water-oil table
S_{org}	Residual oil saturation for liquid-gas table
S_{orw}	Residual oil saturation for water-oil table
$\mathbf{S_w}$	Water saturation
S_{wcrit}	Critical water saturation
Abbreviations	
CMG	Computer Modelling Group Ltd.
CO_2	Carbon dioxide
COBR	Crude Oil/Brine/Rock
CSWI	Carbonated Smart Water Injection
CSW	Carbonated Smart Water
CW	Carbonated Water
CWI	Carbonated Water Injection
DECE	Designed Exploration and Controlled Evolution
DTRAPNA	Relative Permeability Interpolation parameter (low capillary number for high IFT)
DTRAPNB	Relative Permeability Interpolation parameter (high capillary number for low IFT)
EOR	Enhanced Oil Recovery
IFT	Interfacial Tension

OIIP	Oil Initial In Place
OPAAT	One Parameter At A Time
Prod BHP	Bottom-Hole-Pressure Production Rate
PSO	Particle Swarm Optimization
PV	Pore Volume
PVT	Pressure, Volume, and Temperature
RBF	Radial Basis Function (Reservoir Simulator)
RSM	Response Surface Methodology
SW/LSW	Smart Water/Low Salinity Water

References

Adel, I.A., Hassan, A.M., Al-Shalabi, & AlAmeri, W. 2023. A Look Ahead to The Future of Surfactant Flooding EOR In Carbonate Reservoirs Under Harsh Conditions of High Temperature and High Salinity. Presented at the Gas & Oil Technology Showcase and Conference, Dubai, UAE. SPE-214154-MS. http://dx.doi.org/10.2118/214154-MS.

Adel, I.A., Zhang, F., Bhatnagar, N.et al. 2018a. The Impact of Gas-Assisted Gravity Drainage on Operating Pressure in a Miscible CO2 Flood. Presented at the SPE Improved Oil Recovery Conference, Tulsa, Oklahoma, USA. SPE-190183-MS. https://doi.org/10.2118/190183-MS.

Adel, I.A., Tovar, F.D., Zhang, F.et al. 2018b. The Impact of Mmp on Recovery Factor During CO_2 – EOR in Unconventional Liquid Reservoirs. Presented at the SPE Annual Technical Conference and Exhibition, Dallas, Texas, USA. 17. SPE-191752-MS. https://doi.org/10.2118/191752-MS.

Akbar, M., Vissapragada, B., Alghamdi, A.H., Allen, D., Herron, M., Carnegie, A., Dutta, D., Olesen, J.R., Chourasiya, R.D., Logan, D., and Stief, D., 2000. A snapshot of carbonate reservoir evaluation. *Oilfield review*, **12** (4): 20–21.

Aljuboori, F.A., Lee, J.H., Elraies, K.A., and Stephen, K.D., 2019. Gravity drainage mechanism in naturally fractured carbonate reservoirs; review and application. *Energies*, **12** (19), pp. 3699.

Alkhatib, A.M. and King, P.R., 2014. The Use of the Least Squares Probabilistic Collocation Method in Decision Making in the Presence of Uncertainty for Chemical EOR Processes. Paper SPE 170587, SPE Annual Technical Conference and Exhibition, Amsterdam, Netherlands.

Al-Shalabi, E.W., Sepehrnoori, K., and Pope, G., 2014. Geochemical investigation of the combined effect of injecting low salinity water and carbon dioxide on carbonate reservoirs. *Energy Procedia*, **63**: 7663–7676.

Al-Shalabi, E.W., Sepehrnoori, K., and Pope, G., 2016. Numerical modeling of combined low salinity water and carbon dioxide in carbonate cores. *Journal of Petroleum Science and Engineering*, **137**: 157–171.

AlSofi, A.M. and Blunt, M.J., 2011. The design and optimization of polymer flooding under uncertainty. Paper SPE 145110, SPE Enhanced Oil Recovery Conference, Kuala Lumpur, Malaysia.

Alvarado, V. and Manrique, E., 2010. Enhanced oil recovery: an update review. *Energies*, **3** (9): 1529–1575.

Ayirala, S.C., Li, Z., Saleh, S.H., Xu, Z., and Yousef, A.A., 2019. Effects of salinity and individual ions on crude-oil/ water interface physicochemical interactions at elevated temperature. *SPE Reservoir Evaluation & Engineering*, **22** (3): 897–910.

Ayirala, S., Saleh, S., Enezi, S., and Yousef, A., 2020. Multiscale Aqueous-ion interactions at interfaces for enhanced understanding of controlled-ionic-composition-waterflooding processes in carbonates. *SPE Reservoir Evaluation & Engineering*, **23** (3): 1118–1132.

Bai, G.P. and Xu, Y., 2014. Giant fields retain dominance in reserves growth. *Oil & Gas Journal*, **112** (2).

Chavan, M., Dandekar, A., Patil, S., and Khataniar, S., 2019. Low-salinity-based enhanced oil recovery literature review and associated screening criteria. *Petroleum Science*, **16** (6): 1344–1360.

Chilingar, G.V. and Yen, T.F., 1983. Some notes on wettability and relative permeabilities of carbonate reservoir rocks, II. *Energy Sources*, **7** (1): 67–75.

Computer Modeling Group (CMG), 2019. *User technical manual.*

Corey, A.T., 1977. *Mechanics of heterogeneous fluids in porous media*. Water Resources Publications.

Douarche, F., Da Veiga, S., Feraille, M., Enchéry, G., Touzani, S., and Barsalou, R., 2014. Sensitivity analysis and optimization of surfactant-polymer flooding under uncertainties. *Oil & Gas Science and Technology–Revue d'IFP Energies nouvelles*, **69** (4): 603–617.

Garcia, D., Arostegui, I., and Prellezo, R., 2019. Robust combination of the Morris and Sobol methods in complex multidimensional models. *Environmental Modelling & Software*, **122**:104517.

Ghosh, B., Al-Hamairi, A., and Jin, S., 2020. Carbonated water injection: an efficient EOR approach. A review of fundamentals and prospects. *Journal of Petroleum Exploration and Production Technology*, **10** (2): 673–685.

Ghosh, B., Kilybay, A., Thomas, N.C., Haroun, M., Rahman, M.M., and Belhaj, H., 2022. Hybrid Carbonated Engineered Water as EOR Solution for Oil-Wet Carbonate Formation. *Energies*, **15** (21), pp. 7889.

Hakiki, F., Maharsi, D.A., and Marhaendrajana, T., 2015. Surfactant-polymer coreflood simulation and uncertainty analysis derived from laboratory study. *J. Eng. Technol. Sci.*, **47**: 706–725.

Hassan, A.M., Tackie-Otoo, B.N., Ayoub, M., Eissa, M., Al-Shalabi, E.W., and Adel, I.A., 2023. Numerical Investigation of Hybrid Smart Water and Foam Injections in Carbonate Reservoirs. In international Petroleum Technology Conference. OnePetro. http://dx.doi.org/10.2118/212663-MS

Hassan, A.M., Ayoub, M., Eissa, M., Al-Shalabi, E.W., Al-Mansour, A., and Al-Quraishi, A., 2022a. Increasing Reservoir Recovery Efficiency through Laboratory-Proven Hybrid Smart Water-Assisted Foam (SWAF) Flooding in Carbonate Reservoirs. *Energies*, **15**(9), p.3058.

Hassan, A.M., Ayoub, M., Eissa, M., Al-Shalabi, E.W., Almansour, A., and Alquraishi, A., 2022b. Foamability and Foam Stability Screening for Smart Water Assisted Foam Flooding: A New Hybrid EOR Method. In International Petroleum Technology Conference. OnePetro.

Hassan, A.M., Ayoub, M.A., Mohyaldinn, M.E. and Al-Shalabi, E.W., 2022c, October. Insights into Hybrid Smart Water Assisted Foam (SWAF) Flooding in Carbonate Reservoirs: A Combined Numerical and Experimental Approach. In *ADIPEC-2022*. OnePetro.

Hassan, A.M., Ayoub, M.A., Mohyadinn, M.E., Al-Shalabi, E.W., and Alakbari, F.S., 2022d. A New Insight into Smart Water Assisted Foam SWAF Technology in Carbonate Rocks using Artificial Neural Networks ANNs. In Offshore Technology Conference Asia. OnePetro.

Hassan, A.M., Ayoub, M.A., Mohyadinn, M.E., Al-Shalabi, E.W., and Alakbari, F.S., 2022e. A New Insight into Smart Water Assisted Foam SWAF Technology in Carbonate Rocks using Artificial Neural Networks ANNs. In Offshore Technology Conference Asia. OnePetro.

Hassan, A., Ayoub, M., Eissa, M., Bruining, H., Al-Mansour, A., and Al-Quraishi, A., 2021. A New Hybrid Improved and Enhanced Oil Recovery IOR/EOR Process Using Smart Water Assisted Foam SWAF Flooding in Carbonate Rocks, A Laboratory Study Approach. In International Petroleum Technology Conference. OnePetro.

Hassan, A., Ayoub, M., Eissa, M., Bruining, H., Al-Mansour, A., and Al-Guraishi, A., 2020a. A Novel Hybrid Enhanced Oil Recovery Method by Smart Water-Injection and Foam-Flooding in Carbonate Reservoirs. In SPE/IATMI Asia Pacific Oil & Gas Conference and Exhibition. OnePetro.

Hassan, A., Ayoub, M., Eissa, M., Bruining, H., Al-Mansour, A., and Al-Guraishi, A., 2020b. A study of combined low salinity foam injection using dlvo theory and surface complexation modeling. In Offshore Technology Conference Asia. OnePetro.

Hassan, A.M., Ayoub, M., Eissa, M., Bruining, H., and Zitha, P., 2020c. Study of surface complexation modeling on a novel hybrid enhanced oil recovery (EOR) method; smart-water assisted foam-flooding. *Journal of Petroleum Science and Engineering*, **195**, p. 107563.

Hassan, A.M., Ayoub, M., Eissa, M., Musa, T., Bruining, H., and Farajzadeh, R., 2019. Exergy return on exergy investment analysis of natural-polymer (Guar-Arabic gum) enhanced oil recovery. *Energy Journal*, **181** (15), pp. 162–172.

Horowitz, B., Guimaraes, L.J., Dantas, V., and Afonso, S.M., 2010. A concurrent efficient global optimization algorithm applied to polymer injection strategies. *J. of Petrol. Sci. and Eng.*, **71** (3): 195–204.

IEA, 2020. *World Energy Outlook.* OECD Publishing.

IEA, 2021. *World Energy Outlook.*

Kumar, A. and Mandal, A., 2020. Core-scale modeling and numerical simulation of zwitterionic surfactant flooding: designing of chemical slug for enhanced oil recovery. *Journal of Petroleum Science and Engineering*, **192**, pp. 107333.

Lager, A., Webb, K.J., Black, C.J.J., Singleton, M., and Sorbie, K.S., 2008b. Low salinity oil recovery-an experimental investigation1. *Petrophysics-The SPWLA Journal of Formation Evaluation and Reservoir Description*, **49** (01).

Lager, A., Webb, K.J., Collins, I.R., and Richmond, D.M., 2008a. LoSal™ enhanced oil recovery: evidence of enhanced oil recovery at the reservoir scale. Paper SPE 113976, *SPE symposium on improved oil recovery*, Tulsa, Oklahoma, USA.

Lake, L., Johns, R.T., Rossen, W.R., and Pope, G.A., 2014. *Fundamentals of enhanced oil recovery.*

Liu, H. and Chen, Z., 2018. A scalable thermal reservoir simulator for Giant models on parallel computers. *arXiv preprint*, arXiv:1812.03952.

Morrow, N.R., 1991. *Interfacial phenomena in petroleum recovery.* NR Morrow (ed.), pp. 77–99.

Riazi, M., Sohrabi, M., Jamiolahmady, M., and Ireland, S., 2009. Oil recovery improvement using CO_2-enriched water injection. *Paper SPE 121170, EUROPEC/EAGE conference and exhibition*, Amsterdam, The Netherlands.

Sohrabi, M., Riazi, M., Jamiolahmady, M., Ireland, S., and Brown, C., 2009. Mechanisms of oil recovery by carbonated water injection. *SCA annual meeting*, pp. 1–12.

Soleimani, P., Shadizadeh, S.R., and Kharrat, R., 2021. Experimental assessment of hybrid smart carbonated water flooding for carbonate reservoirs. *Petroleum*, **7** (1): 80–90.

Tetteh, J.T. and Barati, R., 2019. Crude-oil/brine interaction as a recovery mechanism for low-salinity waterflooding of carbonate reservoirs. *SPE Reservoir Evaluation & Engineering*, **22** (3): 877–896.

Webb, K.J., Black, C.A., and Al-Ajeel, H., 2004. Low salinity oil recovery-log-inject-log. Paper SPE 81460, SPE/DOE Symposium on Improved Oil Recovery, Bahrain.

Yongmao, H., Zenggui, W., Binshan, J., Yueming, C., and Xiangjie, L., 2004. Laboratory investigation of CO_2 flooding. Paper SPE 88883, Nigeria Annual International Conference and Exhibition, Abuja, Nigeria.

Yousef, A.A., Al-Saleh, S., and Al-Jawfi, M., 2011. New recovery method for carbonate reservoirs through tuning the injection water salinity: Smart waterflooding. Paper SPE 143550, SPE EUROPEC/EAGE annual conference and exhibition, Vienna, Austria.

Zainal, S., Manap, A.A.A., Hamid, P.A., Othman, M., Chong, M.B.O., Yahaya, A.W., Darman, N.B., and Mat Sai, R., 2008. Offshore Chemical EOR: The Role of an Innovative Laboratory Program in Managing Result Uncertainty to Ensure the Success of a Pilot Field Implementation. Paper SPE 113154, Europec/EAGE Conference and Exhibition, Rome, Italy.

Zerpa, L.E., Queipo, N.V., Pintos, S., Tillero, E., and Alter, D., 2007. An efficient response surfaces approach for the optimization of ASP flooding processes: ASP pilot project LL-03 reservoir. Paper SPE 107847, SPE Latin America and Caribbean Petroleum Engineering Conference, Buenos Aires, Argentina.

Zhang, F., Saputra, I.W., Adel, I.A., and Schechter, D.S., 2019. Numerical Investigation of EOR Applications in Unconventional Liquid Reservoirs through Surfactant-Assisted Spontaneous Imbibition SASI and Gas Injection Following Primary Depletion. Paper SPE 196055, SPE Annual Technical Conference and Exhibition, Calgary, Alberta, Canada.

Zhang, F., Adel, I. A., Saputra, I. W. R.et al. 2019a. Numerical Investigation to Understand the Mechanisms of CO2 EOR in Unconventional Liquid Reservoirs. Paper presented at the SPE Annual Technical Conference and Exhibition, Calgary, Alberta, Canada. SPE-196019-MS. https://doi.org/10.2118/196019-MS.

Zhang, F., Saputra, I.W.R., Adel, I.A.et al. 2019b. Numerical Investigation of EOR Applications in Unconventional Liquid Reservoirs through Surfactant-Assisted Spontaneous Imbibition (Sasi) and Gas Injection Following Primary Depletion. Presented at the SPE Annual Technical Conference and Exhibition, Calgary, Albert, Canada. SPE-196055-MS. https://doi.org/10.2118/196055-MS

Webb, K.J., Black, C.A. and Al-Ajeel, H., 2004, April. Low salinity oil recovery-log-inject-log. In SPE/DOE Symposium on Improved Oil Recovery. OnePetro.

Appendix A

Sensitivity Analysis Data (PSO: Particle Swarm Optimization)

Objective Function Name: CumOil

Model Classification: Reduced Quadratic (alpha=0.1) (R2-training=0.986, R2-verification = 0.999)

Table A-1—Summary of fit

R-Square	0.985674
R-Square Adjusted	0.983069
R-Square Prediction	0.977562
Mean of Response	8.30365
Standard Error	0.336966

Table A-2—Analysis of varianc e

Source	Degrees of Freedom	Sum of Squares	Mean Square	F Ratio	Prob > F
Model	6	257.805	42.9675	378.415	<0.00001
Error	33	3.74702	0.113546		
Total	39	261.552			

Table A-3—Effect screening using normalized parameters (-1, +1)

Term	Coefficient	Standard Error	t Ratio	Prob > |t|	VIF
Intercept	8.19709	0.0812996	100.826	<0.00001	0.00
DTRAP(0.0072, 0.012)	0.0258051	0.0880068	0.293217	0.77119	1.04
NG(1.5, 2.5)	0.141308	0.088235	1.60149	0.11880	1.08
Poro(0.166125, 0.276875)	1.90297	0.0854279	22.2757	<0.00001	1.08
Soi(0.50925, 0.84875)	3.23168	0.0925099	34.9333	<0.00001	1.21
Swi(0.24075, 0.40125)	0.234416	0.0868868	2.69795	0.01091	1.03
DTRAP*DTRAP	0.218978	0.158363	1.38276	0.17602	1.07

Table A-4—Coefficients in terms of actual parameters

Term	Coefficient
Intercept	-10.444
DTRAP	-719.174
NG	0.282615
Poro	34.3651
Soi	19.0379
Swi	2.92108
DTRAP*DTRAP	38017

Equation in Terms of Actual Parameters

CumOil=-10.444-719.174*DTRAP+0.282615*NG+34.3651*Poro+19.0379*Soi+2.92108*Swi +38017*DTRAP*DTRAP.

Appendix B

History Matching Data (PSO: Particle Swarm Optimization)

Objective Function Name: GlobalHmError
Model Classification: Reduced Quadratic (alpha=0.1) (R2-training=0.800)

Table B-1—Summary of fit

R-Square	0.799753
R-Square Adjusted	0.793119
R-Square Prediction	0.709165
Mean of Response	12.0259
Standard Error	2.89622

Table B-2—Analysis of varianc e

Source	Degrees of Freedom	Sum of Squares	Mean Square	F Ratio	Prob > F
Model	16	16180.7	1011.3	120.563	<0.00001
Error	483	4051.44	8.38808		
Total	499	20232.2			

Table B-3—Effect screening using normalized parameters (−1, +1)

Term	Coefficient	Standard Error	t Ratio	Prob > |t|	VIF
Intercept	15.5139	0.796225	19.4844	<0.00001	0.00
DTRAP(0.0072, 0.012)	4.00368	0.722417	5.54207	<0.00001	3.31
KRGCL(0.6, 1)	2.51649	0.68411	3.67849	0.00026	2.88
NG(1.5, 2.5)	−1.19238	0.535867	−2.22514	0.02653	1.86
NOG(1.5, 2.5)	2.95338	0.630549	4.68383	<0.00001	2.61
SGCRIT(0.0375, 0.0625)	−2.25802	0.456223	−4.94938	<0.00001	1.37
SORG(0.075, 0.125)	3.00028	0.613304	4.89199	<0.00001	2.52
SORW(0.225, 0.375)	−0.768887	0.495631	−1.55133	0.12148	1.27
Soi(0.50925, 0.84875)	10.0997	0.67201	15.0292	<0.00001	1.41
Swi(0.24075, 0.40125)	3.40464	0.612737	5.55646	<0.00001	2.32
DTRAP*DTRAP	2.64668	0.714209	3.70575	0.00024	2.06
KRGCL*KRGCL	−2.77433	0.733065	−3.78456	0.00017	2.37
NOG*NOG	3.1267	0.710612	4.40002	0.00001	2.40
SGCRIT*SGCRIT	1.76716	0.957421	1.84575	0.06554	1.70
SORG*SORG	−2.81517	0.652308	−4.31571	0.00002	2.14
SORW*SORW	5.58561	0.987138	5.65839	<0.00001	1.59
Soi*Soi	22.2057	1.11124	19.9829	<0.00001	1.53

Table B-4—Coefficients in terms of actual parameters

Term	Coefficient
Intercept	404.356
DTRAP	−7154.07
KRGCL	123.556
NG	−2.38476
NOG	−44.1205
SGCRIT	−1311.62
SORG	1020.87
SORW	−606.05
Soi	−987.015
Swi	42.4255
DTRAP*DTRAP	459493
KRGCL*KRGCL	−69.3582
NOG*NOG	12.5068
SGCRIT*SGCRIT	11309.8
SORG*SORG	−4504.28
SORW*SORW	992.997
Soi*Soi	770.628

Equation in Terms of Actual Parameters

GlobalHmError = 404.356-7154.07*DTRAP+123.556*KRGCL-2.38476*NG-44.1205*NOG-1311.62*SGCRIT+1020.87*SORG-606.05*SORW-987.015*Soi+42.4255*Swi +459493*DTRAP*DTRAP-69.3582*KRGCL*KRGCL+12.5068*NOG*NOG+11309.8*SGCRIT*SGCRIT-4504.28*SORG*SORG+992.997*SORW*SORW+770.628*Soi*Soi

Appendix C

Optimization Progress Data (PSO: Particle Swarm Optimization)

Objective Function Name: OilRecoveryFactor
Model Classification: Reduced Quadratic (alpha=0.1) (R2-training=0.496)

Table C-1—Summary of fit

R-Square	**0.496499**
R-Square Adjusted	0.492430
R-Square Prediction	0.451326
Mean of Response	55.4168
Standard Error	0.00434277

Table C-2—Analysis of variance

Source	Degrees of Freedom	Sum of Squares	Mean Square	F Ratio	Prob > F
Model	4	0.00920569	0.00230142	122.029	<0.00001
Error	495	0.0093355	1.88596E-05		
Total	499	0.0185412			

Table C-3—Effect screening using normalized parameters (-1, +1)

Term	Coefficient	Standard Error	t Ratio	Prob < |t|	VIF
Intercept	55.3993	0.00095636	57927.2	<0.00001	0.00
MinWater(0.656478, 0.9)	−0.00782098	0.0015434	−5.06736	<0.00001	2.89
MaxCO2(0.075, 0.5)	0.0222633	0.00153369	14.5162	<0.00001	2.52
MinWater*MinWater	−0.00520486	0.00132756	−3.92063	0.00010	2.57
MaxCO2*MaxCO2	−0.00520154	0.00136828	−3.80152	0.00016	2.22

Table C-4—Coefficients in terms of actual parameters

Term	Coefficient
Intercept	55.197
MinWater	0.482199
MaxCO2	0.171003
MinWater*MinWater	−0.351069
MaxCO2*MaxCO2	−0.11519

Equation in Terms of Actual Parameters

OilRecoveryFactor=55.197+0.482199*MinWater
+0.171003*MaxCO2-0.351069*MinWater*MinWater-0.11519*MaxCO2*MaxCO2